natureresearch

https://doi.org/10.1038/s41565-020-0770-x

Supplementary information

Optical fibres with embedded two-dimensional materials for ultrahigh nonlinearity

In the format provided by the authors and unedited

Supplementary Information for

Optical fibres with embedded two-dimensional materials for ultrahigh nonlinearity

Yonggang Zuo, Wentao Yu, Can Liu, Xu Cheng, Ruixi Qiao, Jing Liang, Xu Zhou, Jinhuan Wang, Muhong Wu, Yun Zhao, Peng Gao, Shiwei Wu, Zhipei Sun, Kaihui Liu, Xuedong Bai, Zhongfan Liu

The supplementary information includes:

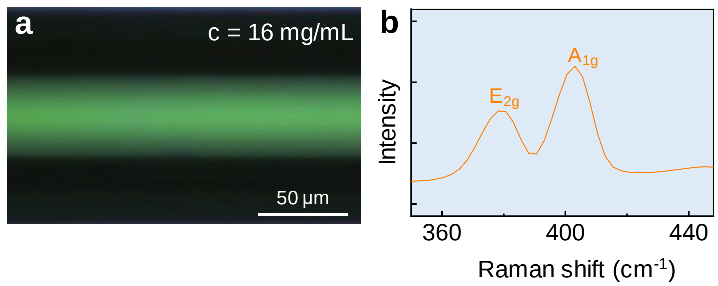

Supplementary Fig. 1 | Few-layered MoS_2 grown on the inner wall of an optical fibre. a, Optical image of MoS_2 embedded fibre synthesized by using a higher Na_2MoO_4 aqueous solution concentration of 16 mg/mL. **b**, Typical Raman spectrum of the MoS_2 film in (a). The frequency difference between A_{1g} and E_{2g} is 22.8 cm^{-1}, revealing the formation of few-layered MoS_2.

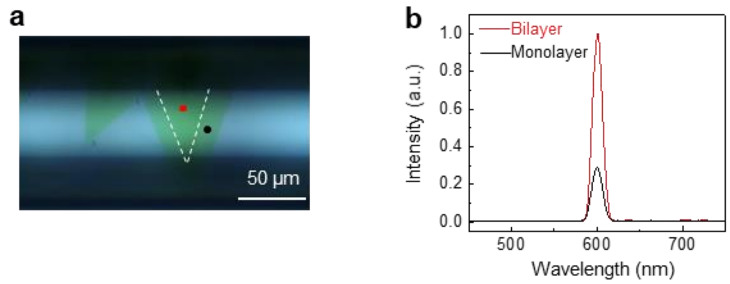

Supplementary Fig. 2 | Measurement on the stacking order of MoS_2 bilayer domains in fibre. **a**, Optical image of MoS_2 bilayer domain. It can be clearly seen that the two layers of MoS_2 are aligned in the same direction. **b**, SHG signals at different locations labelled in (a). The ~4 times SHG enhancement of bilayer region confirms that the stacking order is AA configuration.

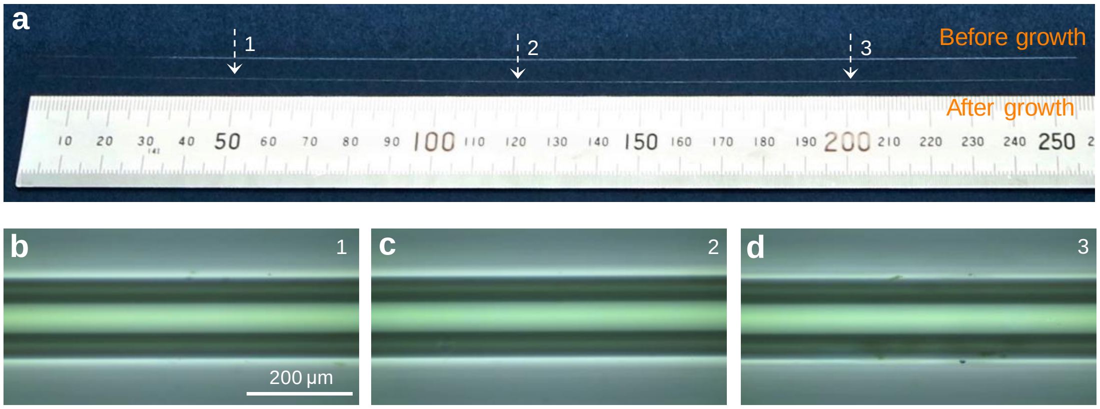

Supplementary Fig. 3 | Uniform MoS_2 growth into a 25-cm-long MoS_2 embedded fibre. a, Typical photograph of the 25-cm-long fibre before and after MoS_2 growth. The colour of fibre turns darker after MoS_2 growth compared with the bare one. **b-d**, Optical images zoomed in at the three positions of MoS_2 embedded fibre labelled in (a), showing the uniformly distributed MoS_2 film along the whole fibre.

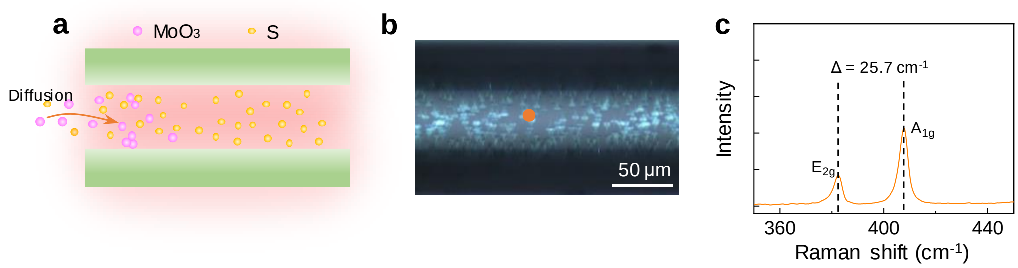

Supplementary Fig. 4 | Controlled experiment of directly sending MoO_3 from outside of the fibres without the pre-deposition step. **a**, Schematic of directly sending MoO_3 and S from outside of the fibres. **b**, Optical image of randomly distributed MoS_2 domains with heterogeneous layer numbers on the entrance side of fibre. **c**, Raman spectrum of MoS_2 domains labelled in (b).

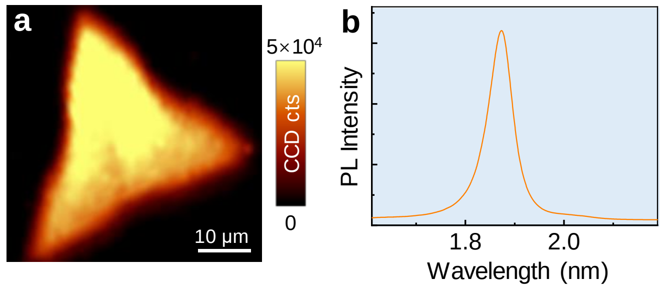

Supplementary Fig. 5 | Photoluminescence (PL) mapping of a MoS_2 domain in optical fibre. **a-b**, A representative PL mapping (a) and spectrum (b) of a triangular MoS_2 sample on the inner wall of fibre. The decreased intensity in the bottom part of (a) arises from the out of focus due to the curvature of fibre hole wall.

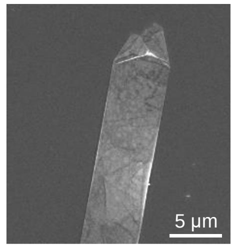

Supplementary Fig. 6 | Scanning electron microscopic (SEM) image of a MoS_2 ribbon. After etching the quartz fibre in hydrofluoric acid, the inner cylindroid MoS_2 film collapsed into a ribbon.

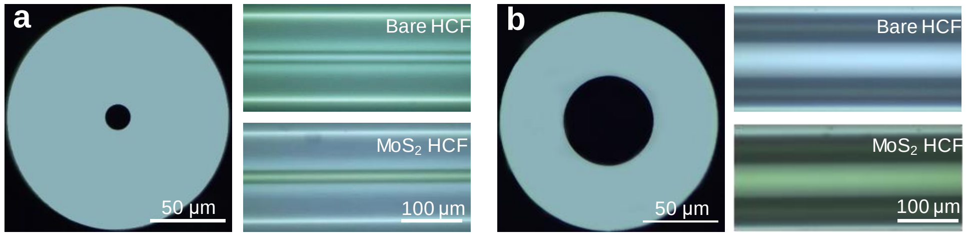

Supplementary Fig. 7 | Optical images of MoS_2 embedded hollow capillary fibre (HCF) with different diameters. a-b, Optical images of the HCF with ~15 µm (a) and ~50 µm (b) hollow cores, respectively. After MoS_2 growth, the fibre cores have higher optical contrast.

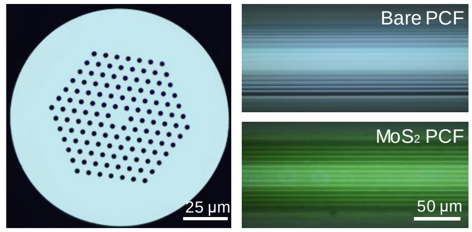

Supplementary Fig. 8 | Optical images of a MoS_2 embedded photonic crystal fibre (PCF) with solid-core honeycomb structure. All holes of PCF were filled with tube-like MoS_2 film, resulting in a green colour compared with bare PCF.

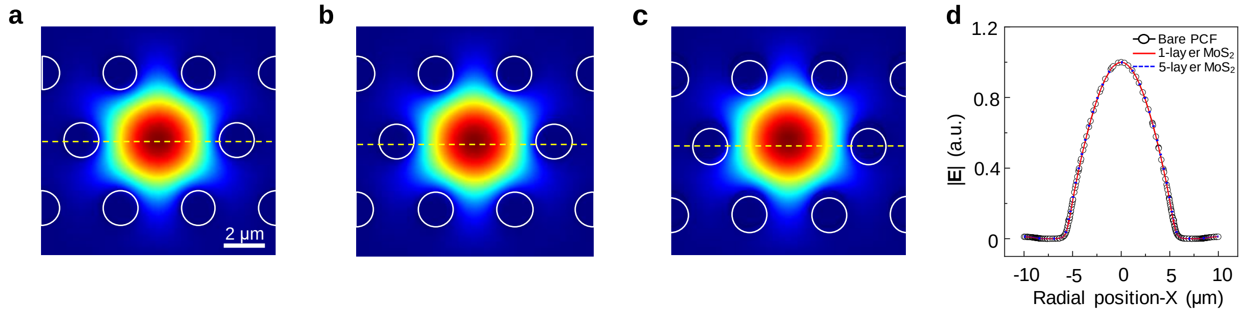

Supplementary Fig. 9 | Distribution of fundamental mode in different photonic crystal fibre (PCF). **a**, Bare PCF. **b**, Monolayer MoS_2 embedded PCF. **c**, Five-layers MoS_2 embedded PCF. **d**, Distribution of the normalized electric field along the horizontal radial direction (yellow dashed lines in (a)-(c)). It is seen that the modes are all well confined in the fibre core region and nearly show the same morphology under different layer numbers of MoS_2. The main reason of this phenomenon lies in that the change of refractive index distribution caused by the atomic layer thickness of 2D materials (nm scale) is negligible for the sub-micrometre-scale fibre structure.

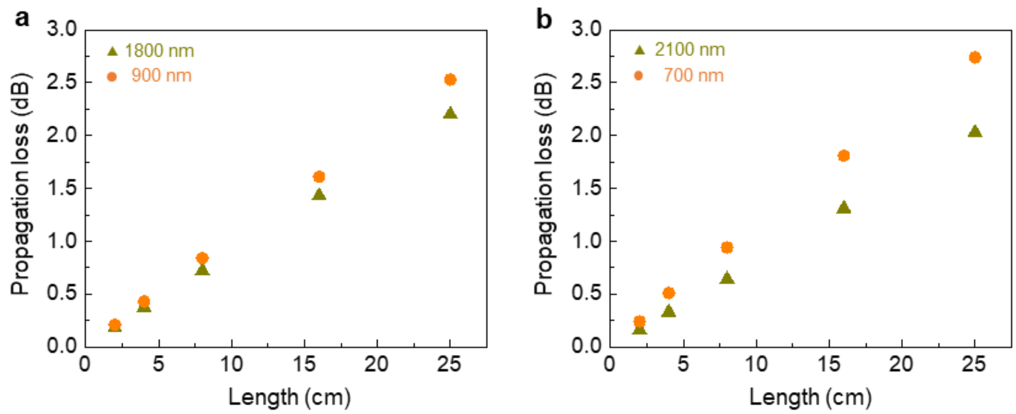

Supplementary Fig. 10 | Propagation loss of MoS_2 embedded fibres with different lengths at different wavelengths. a, 0.090 dB/cm for fundamental wavelength of 1800 nm and 0.097 dB/cm for SHG wavelength of 900 nm. **b**, 0.085 dB/cm for fundamental wavelength of 2100 nm and 0.11 dB/cm for THG wavelength of 700 nm. Both the excited and emitted signals have very weak losses and guaranteed the enough light-material interaction for maximum nonlinear signal.

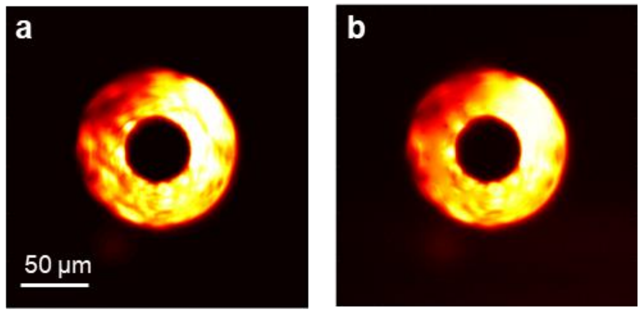

Supplementary Fig. 11 | Optical images of the nonlinear signal output from the MoS_2 capillary. **a**, SHG image with excited wavelength of 1800 nm. **b**, THG image with excited wavelength of 2100 nm.

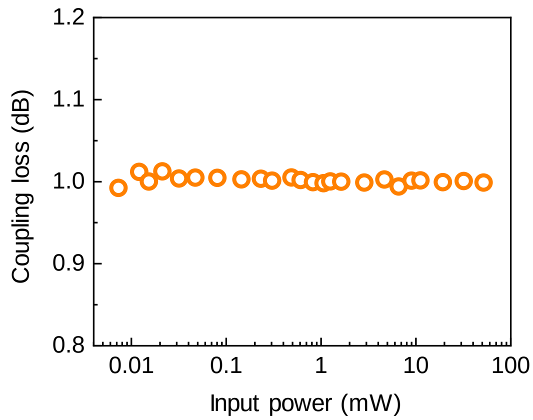

Supplementary Fig. 12 | Measured coupling loss of bare photonics crystal fibre (PCF) aligned with single mode fibre under different input laser powers. The low coupling loss (~1dB) attributes to the similar mode diameters of HC1550 and SM-28e+, and can be acceptable in the all-fibre devices.

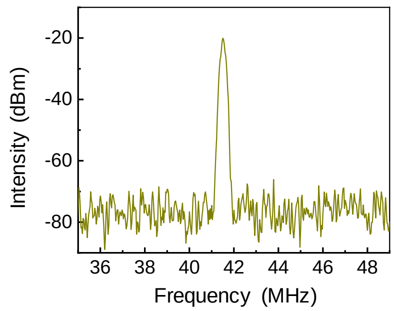

Supplementary Fig. 13 | Characterization of the output pulse train of fibre laser based on MoS_2 embedded photonic crystal fibre. Radio frequency spectrum of the pulse train with a centre frequency of ~41 MHz and a high signal-to-noise ratio of ~52 dB.

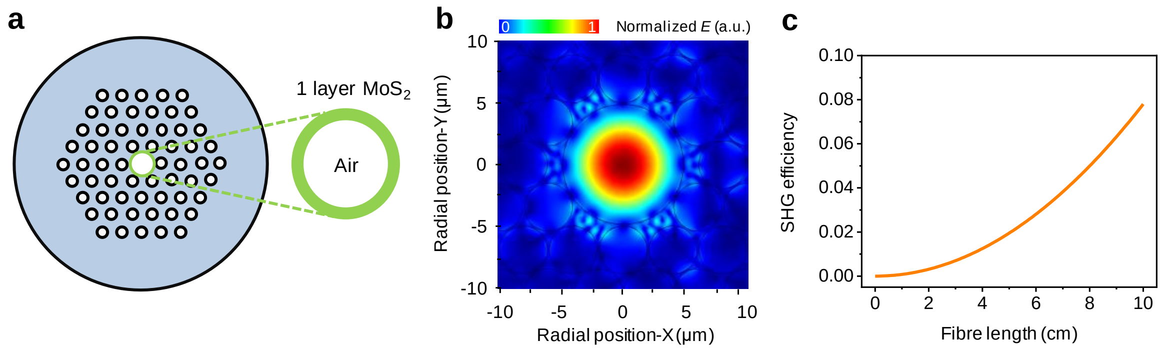

Supplementary Fig. 14 | The simulation conversion efficiency of second harmonic generation (SHG) in MoS_2 embedded photonic crystal fibre (PCF). a, The schematic diagrams of MoS_2 PCF. **b**, The normalized calculated electric field distribution of the fundamental guided mode in MoS_2 PCF with light wavelength of 1800 nm. **c**, The simulation conversion efficiency of SHG in MoS_2 PCF with different fibre lengths under the condition of phase matching between pump and SHG light. The efficiency can reach ~8% with the fibre length of 10 cm.

Supplementary Table 1. Comparisons of nonlinear performance of optical fibres integrated with 2D materials by different methods

Table R1 ｜Comparisons of nonlinear performance of optical fibres integrated with 2D materials by different methods					
Integration fibre types	**2D materials**	**Interaction length**	**Nonlinear process**	**Efficiency or enhancement**	**References**
D-shaped fibre	Black phosphorus	Centimeter-scale	FWM	33% enhancement	1
Taped fibre	Graphene	~1 cm	FWM	1% efficiency	2
	GaAs	~4 mm	SHG	10000 times enhancement compared with bare taped fibre	3
Fibre nanowire	WS_2	0.1 mm	SHG	20 times enhancement compared with bare fibre nanowire	4
Direct growth in fibre holes	MoS_2	~25 cm	SHG/THG	1000 times enhancement compared with pristine MoS_2	This work

Note: FWM, four-wave mixing; SHG, second harmonic generation; THG, third harmonic generation

Supplementary Table 2. Comparisons of ultra-fast laser based on optical fibres integrated with MoS_2 by different methods

Table R2 ｜Comparisons of ultra-fast lasers based on different fibre SAs integrated with MoS_2					
Integration method	**Light-matter coupling mode**	**Fabrication method**	**Pulse width**	**Repeatability and batch manufacture**	**References**
Fibre facet	Direct coupling	Growth and transfer	250 fs, 1.28 ps	Bad	5,6
		LPE and coating	1.55 ns, 90 ns	Good	7,8
D-shaped or taped fibre	Evanescent wave coupling	Growth and transfer	521 fs, 637 fs, ~1 ps	Bad	9-11
		LPE and coating	1.21 ps, ~3 ps, 12.7 ps	Good	12-14
Direct growth in fibre holes	Evanescent wave coupling	Direct CVD growth	500 fs	Good	This work

Note: CVD, chemical vapour deposition; LPE, liquid phase exfoliation

Supplementary Note 1: Diffusion of the feedstocks in the fibre holes

In our designed two-step CVD growth method, two kinds of feedstocks (Na_2MoO_4 and sulphur) are supplied for the deposition of MoS_2 on the holes of fibre. Since Na_2MoO_4 feedstock was already pre-deposited onto the inner walls, and would release Mo precursors slowly and continuously by vaporization, there was always sufficient Mo precursors supply in the confined space of fibre holes. However, the sulphur vapour was brought in from the upstream to the holes of fibre, in which the diffusion process should be seriously considered in our design.

It has been reported that sulphur is mainly diffused in the form of S_2 in the CVD system[15]. According to thermodynamics, the mean-free-path (λ_m) of gaseous S_2 moleculars in our experiment condition is

$$\lambda_m = \frac{kT}{\sqrt{2}\pi P d^2} = 630\ \mu\text{m}, \tag{1.1}$$

where k is the Boltzmann constant, $T = 1100$ K is the experimental temperature, $d = 0.189$ nm is the diameter of S_2 molecular and P = 150 Pa is the pressure of the system. In our experiment, the diameters of holes are in the range of 5 μm to 50 μm, therefore the Knudsen number (K_n) is in the range of ~13-130, which confirms that the diffusion of S_2 molecular virtually belongs to free molecular flow in all of our cases (for free molecular flow, $K_n > 10$)[16].

In a free molecular flow, the velocity distribution of molecule motion is generally uniform and constant. And the average velocity of S_2 molecular motion is

$$< v_m > = \sqrt{3kT/m} = 0.65 \times 10^3\ m/s, \tag{1.2}$$

where m is the mass of the S_2 molecular. So, the collision frequency between molecules can be estimated as

$$f = < v_m > / \lambda_m = 1.0 \times 10^6\ \text{Hz}. \tag{1.3}$$

A S_2 molecule to diffuse out of the fibre should travel a distance of l (~25 cm), therefore the average time for S_2 to diffuse out of the fibre is

$$t = 1/f \times (l/\lambda_m)^2 = 0.15\ s. \quad (1.4)$$

Such short diffusive duration could guarantee S_2 to pass through the holes of fibre effectively and could provide sufficient and homogenous sulphur gas supply for fibres with different diameter sizes we used here.

Supplementary Note 2: Nonlinear energy conversion efficiency of MoS_2 embedded fibre

The energy conversion of the harmonic generation can be described as

$$\eta_c = \frac{P_{nl}}{P_{in}}, \tag{2.1}$$

where P_{nl} and P_{in} are the powers of the nonlinear signal and the input laser, respectively.

In our experiment, the power of the nonlinear signal (P_{nl}) can be described as

$$P_{nl} = \frac{NE}{TG\eta_t\eta_g}, \tag{2.2}$$

where N is the total count from the CCD equipped with the spectrometer, T is the integration time, E is the single photon energy, G is the photon-to-count conversion gain, η_t is the whole transmission efficiency of the collecting light path and η_g is the diffraction efficiency of the grating in the spectrometer. Besides, the power of input laser (P_{in}) can be directly measured using a power meter.

So the final energy conversion can be derived as

$$\eta_c = \frac{NE}{TG\eta_t\eta_g P_{in}}. \tag{2.3}$$

The final energy conversion of our 2D material embedded fibre can reach 10^{-4} to 10^{-3}, which is two or three orders of magnitude higher than previous works[17-19].

Supplementary Note 3: Calculations of the SHG conversion efficiency in MoS_2 embedded fibre

The conversion efficiency of SHG in MoS_2 embedded fibre can be obtained by

$$\eta_{SHG} = \frac{P_{\omega_2}}{P_{\omega_1}} = \frac{\iint I_2 ds_2}{\iint I_1 ds_1}, \tag{3.1}$$

where P_1, I_1, s_1 and P_2 , I_2, s_2 are the power, intensity and area of light input and second harmonic output, respectively. The intensity of light can be expressed as

$$I = \frac{1}{2}\varepsilon_0 cn|E|^2. \tag{3.2}$$

From nonlinear coupled wave equations, under the small signal approximation and off-resonance condition, the electric field intensity of the SHG signal is given by[20,21]

$$\frac{dE_2}{dz} = -\frac{i\omega_2}{2cn_2}\chi^{(2)}E_1^2 e^{-i\Delta kL}, \tag{3.3}$$

so

$$E_2(L) = -\frac{i\omega_2}{2cn_2}\chi^{(2)}E_1^2\frac{e^{-i\Delta kL}-1}{\Delta kL}L. \tag{3.4}$$

Here ω_1, E_1, n_1 and ω_2, E_2, n_2 are the frequency, electric field intensity and refractive index of input light and output second harmonic signal ($\omega_2 = 2\omega_1$), respectively, $\chi^{(2)}$ is second-order nonlinear susceptibility of monolayer MoS_2[22], L is the length of optical fibre, $\Delta k = k_2 - 2k_1$. Using the equations (1) to (4), we can get the SHG conversion efficiency as

$$\eta_{SHG} = \frac{\omega_1^2 \cdot \left[\chi^{(2)}\right]^2 \cdot L^2}{c^2 n^2}\left(\frac{e^{-i\Delta kL}-1}{\Delta kL}\right)^2 \frac{\iint |E_1|^4 ds_1}{\iint |E_1|^2 ds_2}, \tag{3.5}$$

where we assumed that $n_1 = n_2 = n$.

To simplify the calculation process, we chose the hollow-core photonic crystal fibre with monolayer MoS_2 on the centre hole surface (Supplementary Fig. 14a) and assumed that the phase matching has been satisfied (Δk = 0). Combining the simulated fundamental mode electric field distribution by the full-vector finite element method and waveguide theory (Supplementary Fig. 14b) and the presupposed data of input pulsed laser: wavelength λ_1 = 1800 nm, average power P = 15 mW (peak power = 1.5 kW), we can get the conversion efficiency of SHG in MoS_2 embedded optical fibre ~ 8% with 10 cm fibre length (Supplementary Fig. 14c).

References

1 Uddin, S., Debnath, P. C., Park, K. Song, Y. W. Nonlinear black phosphorus for ultrafast optical switching. *Sci. Rep.* **7,** 43371 (2017).

2 Wu, Y. et al. Generation of cascaded four-wave-mixing with graphene-coated microfiber. *Photon. Res.***3,** A64-A68 (2015).

3 Jiang, B. et al. High-efficiency second-order nonlinear processes in an optical microfibre assisted by few-layer GaSe. *Light Sci. Appl.* **9,** 63 (2020).

4 Chen, J. H. et al. Tunable and enhanced light emission in hybrid WS_2-optical-fiber-nanowire structures. *Light Sci. Appl.* **8,** 8 (2019).

5 Xia, H. D. et al. Ultrafast erbium-doped fiber laser mode-locked by a CVD-grown molybdenum disulfide (MoS_2) saturable absorber. *Opt. Express* **22,** 17341-17348 (2014).

6 Xia, H. D. et al. Few-layer MoS_2 grown by chemical vapor deposition as a passive Q-switcher for tunable erbium-doped fiber lasers. *Photon. Res.* **3,** A92-A96 (2015).

7 Sathiyan, S., Velmurugan, V., Senthilnathan, K., Babu, P. R. Sivabalan, S. All-normal dispersion passively mode-locked Yb-doped fiber laser using MoS_2-PVA saturable absorber. *Laser Phys.* **26,** 055103 (2016).

8 Ahmed, M. H. M., Latiff, A. A., Arof, H. Harun, S. W. Mode-locking pulse generation with MoS_2-PVA saturable absorber in both anomalous and ultra-long normal dispersion regimes. *Appl. Opt.* **55,** 4247-4252 (2016).

9 Khazaeinezhad, R. et al. Mode-locked all-fiber lasers at both anomalous and normal dispersion regimes based on spin-coated MoS_2 nano-sheets on a side-polished fiber. *IEEE Photon. J.* **7,** 1500109 (2015).

10 Khazaeizhad, R., Kassani, S. H., Jeong, H., Yeom, D. I. Oh, K. Mode-locking of Er-doped fiber laser using a multilayer MoS_2 thin film as a saturable absorber in both anomalous and normal dispersion regimes. *Opt. Express* **22,** 23732-23742 (2014).

11 Cui, Y. D., Lu, F. F., Liu, X. M. MoS_2-clad microfibre laser delivering conventional, dispersion-managed and dissipative solitons. *Sci. Rep.* **6,** 30524 (2016).

12 Liu, M. et al. Microfiber-based few-layer MoS_2 saturable absorber for 2.5 GHz passively harmonic mode-locked fiber laser. *Opt. Express* **22,** 22841-22846 (2014).

13 Feng, C. et al. Passively mode-locked Nd^{3+}:YVO_4 laser using a molybdenum disulfide as saturable absorber. *Opt. Mater. Express* **6,** 1358-1366 (2016).

14 Wang, Y. D. et al. Harmonic mode locking of bound-state solitons fiber laser based on MoS_2 saturable absorber. *Opt. Express* **23,** 205-210 (2015).

15 Misawa, M. et al. Reactivity of sulfur molecules on MoO_3 (010) surface. *J. Phys. Chem. Lett.* **8,** 6206-6210 (2017).

16 M. Knudsen, *The Kinetic Theory of Gases* (Methuen, London, 1952).

17 Cheng, T. L. et al. Widely tunable second-harmonic generation in a chalcogenide-tellurite hybrid optical fiber. *Opt. Lett.* **39,** 2145-2147 (2014).

18 Yuan, J. H. et al. Generation of second-harmonics near ultraviolet wavelengths from femtosecond pump pulses. *IEEE Photon. Tech. Lett.* **28,** 1719-1722 (2016).

19 Yuan, J. H. et al. Deep-ultraviolet second-harmonic generation by combined degenerate four-wave mixing and surface nonlinearity polarization in photonic crystal fiber. *Sci. Rep.* **7,** 9224 (2017).

20 Shen, Y.-R., *The Principles of Nonlinear Optics* (Wiley, New York, 1984).

21 Yariv, A.,Yeh, P., *Photonics: Optical Electronics in Modern Communications* (Oxford Univ. Press, Oxford, 2006).

22 Autere, A. et al. Nonlinear optics with 2D layered materials. *Adv. Mater.* **30,** 1705963 (2018).